ELSEVIER

International Journal of Heat and Fluid Flow 19 (1998) 69–78

International Journal of HEAT AND FLUID FLOW

Laminar flow efficiency of stratified chilled-water storage tanks

K.O. Homan [a,*], S.L. Soo [b]

[a] Department of Mechanical Engineering, University of Nebraska-Lincoln, 104 N. Walter Scott Engineering, Lincoln, NE 68588-0656, USA
[b] Department of Mechanical and Industrial Engineering, University of Illinois at Urbana-Champaign, Urbana, IL 61801, USA

Received 3 February 1997; accepted 19 August 1997

Abstract

This paper presents results for the efficiency of a stratified chilled-water storage tank with one inlet and one outlet. Numerical solutions for the two-dimensional, unsteady, laminar flow during stably stratified tank filling are compared with a one-dimensional model involving only conductive heat transfer across the thermocline separating the entering cold water and the exiting warm water. This one-dimensional model represents the minimum level of thermal mixing. The difference between the one-dimensional and two-dimensional models are revealed by a horizontal average of the governing equation for the two-dimensional model. Comparison reveals that for inlet Reynolds numbers of approximately 100, the efficiency of the actual, two-dimensional filling is less than 10% below the optimal efficiency of the model. Examination of an effective diffusivity, which can be associated with the mixing ignored in the one-dimensional model, reveals that the early and late stages of the tank-filling process are responsible for most of the deviation between the actual and ideal performances. For the present Reynolds number range, the two-dimensional predictions for effective diffusivity agree well with values derived from published experimental data.

Keywords: Chilled-water storage; Stratified flow; Laminar unsteady mixing

Notation

(Dimensional and dimensionless variables are denoted with and without a hat, respectively.)

c	specific heat (kJ/kg · °C)
COP	coefficient of performance
Fr	Froude number ($\bar{u}/\sqrt{g'l}$)
g, g'	gravitational constant, reduced gravity (m/s^2)
$\mathscr{H}$	operator defined in Eq. (15)
l	inlet height (m)
Q	dimensionless heat transfer
Pe	Peclet number ($\bar{u}l/\alpha$ = Pr Re)
Pr	Prandtl number
Re	Reynolds number ($\bar{u}l/\nu$)
t	dimensionless time ($\hat{t}\bar{u}/l$)
T	dimensionless temperature difference $[(\hat{T}-\hat{T}_i)/\Delta\hat{T}]$
$\overline{T}$	horizontally averaged dimensionless temperature difference
u, v	dimensionless velocity components ($\hat{u}/\bar{u}$, $\hat{v}/\bar{u}$)
$\bar{u}$	average dimensional inlet velocity (m/s)
V	volume (m^3)
W, H	domain width, domain height (m)
x, y	dimensionless Cartesian coordinates ($\hat{x}/l$, $\hat{y}/l$)
Δx, Δy	dimensionless numerical grid size ($\Delta\hat{x}/l$, $\Delta\hat{y}/l$)
y_f	dimensionless elevation of the fill line (t/X)
X, Y	dimensionless domain width, height (W/l, H/l)

Greek

α	molecular thermal diffusivity (m^2/s)
β	thermal expansion coefficient (K^{-1})
δ	dimensionless thermocline half-thickness ($\hat{\delta}/l$)
ε	effective thermal diffusivity (m^2/s)
η	storage tank efficiency
κ	mixing factor
ν	kinematic viscosity (m^2/s)
ρ	density (kg/m^3)
ϕ	dimensionless cold water volume ($\hat{\phi}/l^2$)
ψ	dimensionless stream function ($\hat{\psi}/\bar{u}l$)
ω	dimensionless vorticity ($\hat{\omega}l/\bar{u}$)

Subscripts

c	charging
d	discharging
i	inlet
m	maximum allowable outlet temperature for discharging
o	bulk-averaged outlet temperature
∞	tall tank

* Corresponding author. E-mail: khoman@unlinfo.unl.edu.

0142-727X/98/$19.00
PII: S0142-727X(97)10003-0

1. Introduction

Chilled-water storage has achieved widespread use over the past decade because of its ability to decouple large, peak cooling loads from the operation of their respective chiller plants. With space cooling now accounting for nearly half of the commercial sector's summer peak demand for electricity (Wendland and Blatt, 1992), the potential benefits of this technology are significant. Shifting electrical demand from on-peak to off-peak hours results in a more uniform demand profile for utilities; thereby raising the efficiency of power generation and transmission. For the consumer, operating costs are reduced because of the lower off-peak utility rates, and capital costs are often reduced because of the smaller chiller needed to meet a time-averaged cooling load. Seeley (1996) estimated that cool storage has resulted in a shift of over 300 megawatts of peak cooling load in the United States since 1992.

Most chilled-water storage systems use a single, naturally stratified tank. Although similar in principle to the storage devices commonly used in solar–thermal systems, chilled-water storage tanks (1) operate with one-tenth the density difference, and (2) have a storage volume over one thousand times larger. However, for both chilled-water and solar–thermal storage, it is the level of mixing between the 'hot' and 'cold' liquid that determines the efficiency of the device.

The first studies of stratified chilled-water storage tanks were almost exclusively experimental in nature. Wildin measured efficiency and temperature profile data for both small-scale and laboratory-scale tanks (Wildin and Truman, 1985; Wildin, 1989; Wildin and Sohn, 1993). Baines et al. (1982) examined laboratory-scale tanks with stratification produced by thermal gradients and salinity gradients. The relatively few numerical simulations of the tank-filling process reported in the literature (Cai et al., 1993; Chan et al., 1983; Valentine and Tannous, 1985) have not resolved the large thermal gradients observed experimentally.

One-dimensional models for the vertical transport of the thermocline through the tank have been used in studies of solar–thermal storage tanks. Cole and Bellinger (1982) used a least-squares fit to experimentally measured temperature profiles in order to determine empirical constants in a one-dimensional formulation. Oppel et al. (1985) introduced a finite-difference based algorithm to solve the one-dimensional convective energy equation for the time-varying flowrates arising in a constant-outlet-temperature solar collector. They also introduced an effective diffusivity to account for the thickening of the thermocline produced by turbulent mixing near the inlet. Later, Zurigat et al. (1991) proposed a correlation for the effective thermal diffusivity in terms of a Reynolds number and a Richardson number. Their correlation factor was computed by a trial-and-error method that attempted to obtain good agreement with temperature profiles measured in the late stages of the filling process. Truman et al. (1985) adapted the basic numerical algorithm of Oppel et al. (1985) to produce a model of stratified chilled-water storage that included the heat capacity of the tank wall. Mixing was accounted for by averaging the temperature over a fixed number of grid points located near the inlet (Truman and Wildin, 1989).

Homan et al. (1996) introduced a method for estimating an effective thermal diffusivity by relating an analytic solution of the one-dimensional energy equation to empirically measured thermocline thicknesses and outlet temperature profiles. In a recent paper (Homan and Soo, 1997) we also conducted accurate, direct numerical simulations of the stably stratified filling process in order to identify basic fluid dynamic phenomena occurring during successive stages of the process. In the present paper, we build on this previous work by using our numerical model of the filling process to compute directly its relationship to the analytic model and to the thermal efficiency of a stratified storage tank under laminar flow conditions.

2. Mathematical formulation

2.1. Multidimensional flow model

The two geometries we have considered are shown in Fig. 1. We have chosen these geometries to examine the dynamics of a stratified inflow for (1) tanks with very large aspect ratios, and (2) tanks with order-one aspect ratios. The two geometries enable us to control the impact of the outlet location as well as to examine the complete charging and discharging process. During the charging process, the tank is filled with cold liquid that enters at the lower corner of the tank, while warm liquid is withdrawn, at an equal rate, at the upper corner of the tank. For the discharge process, the role of the inlet and outlet are reversed: warm fluid flows into the tank at the upper boundary or corner of the tank and cold liquid is withdrawn at the lower corner of the tank.

The characteristic length, velocity and time scales have been chosen as the charging inlet height l, the area-averaged inlet velocity $\bar{u}$, and convective time scale $l/\bar{u}$, respectively. With this choice of time scale, a single unit of dimensionless time

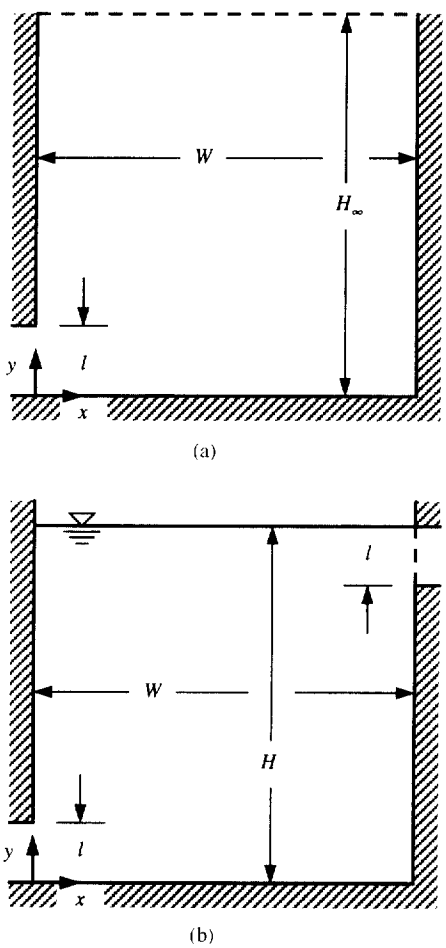

Fig. 1. Geometry and coordinate system for (a) the lower portion of a tall tank with a single corner inlet, and (b) a tank with a single inlet and outlet.

corresponds to the period required for an l^2 'volume' of fluid to flow into or out of the tank. The characteristic temperature difference, $\Delta\hat{T}$, has been chosen as the difference between the initial uniform temperature in the tank and the steady inlet temperature. In the charging process, these temperatures correspond to the minimum and maximum densities, respectively. For the discharging process, the reverse is true: the steady inlet temperature corresponds to the minimum density, and the cold liquid initially in the tank has the maximum density. For an unsteady, two-dimensional flow, the dimensionless vorticity, stream function and energy equations are

$$\nabla^2\psi = -\omega, \tag{1a}$$

$$\frac{\mathrm{d}\omega}{\mathrm{d}t} = \frac{1}{\mathrm{Re}}\nabla^2\omega + \frac{1}{\mathrm{Fr}^2}\frac{\partial T}{\partial x}, \tag{1b}$$

$$\frac{\mathrm{d}T}{\mathrm{d}t} = \frac{1}{\mathrm{Pr}\,\mathrm{Re}}\nabla^2 T, \tag{1c}$$

where $\mathrm{d}/\mathrm{d}t$ denotes the convective derivative. The dimensionless domain is defined by $0 \leqslant x \leqslant X$ and $0 \leqslant y \leqslant Y$. The Reynolds number and Froude number appearing in Eqs. (1a)–(1c) are $\mathrm{Re} \equiv \bar{u}l/\nu$ and $\mathrm{Fr} \equiv \bar{u}/\sqrt{g'l}$, where $g' \equiv g(\Delta\rho/\rho) \cong g(\beta\Delta\hat{T})$ is the reduced internal gravity. The stream function, ψ, and vorticity, ω, are related to the x and y components of velocity by $u = \psi_y$, $v = -\psi_x$ and $\omega = v_x - u_y$, where the subscripts x and y denote differentiation.

We assume a parabolic profile for the horizontal velocity at the inlet. For the charging process, this boundary condition is $u = 6y(1-y)$. The steady inlet temperature is set to zero or one for the charging or discharging process, respectively. Both the inlet conditions on velocity and on temperature are ramped from their initial value to their steady-state value using a cubic startup function over a dimensionless period of 0.2. The conditions applied along the outflow boundary are $\psi_{nn} = 0$, $\omega_n = 0$ and $T_n = 0$, where the subscript n denotes differentiation with respect to the coordinate normal to the boundary. No-slip and adiabatic boundary conditions are enforced on the tank walls. The free surface shown in Fig. 1(b) is modeled as a fixed, horizontal shear-free boundary. This is appropriate because the Froude number based on g, rather than g', is very small. The initial conditions are $\psi = \omega = 0$ and dimensionless temperature equal to 1 or 0 for the charging or discharging process, respectively.

The governing equations, (1a)–(1c), are solved on a grid with uniform spacing in both coordinate directions. For the interior of the domain, the accuracy of the finite-difference scheme is second order in space and first order in time. The vorticity at a solid-wall boundary is computed from a formula that is first-order accurate in space and time. A more detailed description of the numerical method and related accuracy issues can be found in our earlier paper (Homan and Soo, 1997). For all the results presented in this paper, a dimensionless grid size, $\Delta x = \Delta y$, of $\frac{1}{16}$ or smaller has been used.

2.2. Diffusion-limit model

Decomposing the temperature into a horizontally averaged component

$$\overline{T}(y,t) = \frac{1}{X}\int_0^X T(x,y,t)\,\mathrm{d}x, \tag{2}$$

and a perturbation, $T'(x,y,t)$, the full temperature field is given by

$$T(x,y,t) = \overline{T}(y,t) + T'(x,y,t). \tag{3}$$

Averaging Eq. (1c) over the tank width and recognizing that the horizontal average of the vertical velocity at any level above the inlet and below the outlet is $1/X$, the equation simplifies to

$$\frac{\partial\overline{T}}{\partial t} + \frac{1}{X}\frac{\partial\overline{T}}{\partial y} = \frac{\partial}{\partial y}\left(\frac{1}{\mathrm{Pe}}\frac{\partial\overline{T}}{\partial y} - \frac{1}{X}\int_0^X v'T'\,\mathrm{d}x\right) \tag{4}$$

using the no-slip and adiabatic boundary conditions for $1 \leqslant y \leqslant Y-1$. Note that in general, the perturbation integral will be a function of both y and t.

As a first approximation, we assume that the perturbation integral is proportional to the gradient of the mean temperature.

$$\frac{\varepsilon}{\bar{u}l}\frac{\partial\overline{T}}{\partial y} = -\frac{1}{X}\int_0^X v'T'\,\mathrm{d}x, \tag{5}$$

thereby simplifying Eq. (4) to

$$\frac{\partial\overline{T}}{\partial t} + \frac{1}{X}\frac{\partial\overline{T}}{\partial y} = \frac{\kappa}{\mathrm{Pe}}\frac{\partial^2\overline{T}}{\partial y^2}, \tag{6}$$

where $\kappa \equiv (1+\varepsilon/\alpha)$. Since any heat transfer between the warm liquid and the cold liquid reduces the efficiency of the charging and discharging processes, and since conductive heat transfer is unavoidable, the one-dimensional solution of Eq. (6) with $\varepsilon = 0$ and $\kappa = 1$ represents the optimal charging and discharging processes with the maximum achievable efficiencies. Clearly, the thermal-mixing diffusivity, ε, will be nonzero for all actual laminar or turbulent flows, and the increased heat transfer will reduce the efficiency.

The well-known solution to Eq. (6) for a constant and uniform value of κ is

$$\overline{T}(y,t) = 1 - (1/2)\,\mathrm{erfc}\left[\frac{y - t/X}{2(\kappa t/\mathrm{Pe})^{1/2}}\right], \tag{7}$$

subject to the boundary conditions $\overline{T}(-\infty,t) = 0$ and $\overline{T}(\infty,t) < \infty$.

2.3. Measures of thermal mixing

The analytic solution given by Eq. (7) is useful not only as a model of the ideal, limiting behavior of stratified storage but also as a means for relating characteristic features of the temperature history to a quantitative measure of thermal mixing. This measure of thermal diffusion, cast either in terms of κ or ε, can be estimated from the two most common types of experimental data measured in stratified thermal-storage tanks: (1) vertical in-tank temperature profiles, and (2) time traces of the tank inlet and outlet temperature. In this section, we relate these two types of data to the one-dimensional model. Their relationship to the results of the two-dimensional, unsteady numerical solutions will be discussed later in this paper.

With respect to a vertical temperature profile, the most obvious measure of thermal mixing is the thickness of the thermocline. Since the transition from the sharp temperature gradient at the center of the thermocline to the gradient far above or below it decays gradually, quantitative measurement of the thermocline thickness requires a definition of its 'edge', in a sense similar to that of the classical boundary layer. We have chosen to define the thermocline thickness as the vertical distance between the locations where $\overline{T} = T_m$ and where $\overline{T} = 1 - T_m$. These correspond to the lower and upper edges of the thermocline, respectively. The choice of the temperature T_m to define the edge of the thermocline is motivated by the maximum allowable outlet temperature dictated by the heat exchanger interface to the cooling load. During the charging

process, the tank is filled with cold water until the outlet temperature drops below T_m and then during the discharging process, cold water can be withdrawn until the outlet temperature rises to T_m (Wildin and Truman, 1985). In general, the maximum allowable outlet temperature is less than 25% of the characteristic temperature difference $\Delta\hat{T}$.

Since the solution given in Eq. (7) is symmetric about the vertical location of the fill line, $y = y_f \equiv t/X$, the thermocline half-thickness is given symbolically by

$$\delta = t/X - y_m = y_{\bar{m}} - t/X, \tag{8}$$

where y_m and $y_{\bar{m}}$ denote the vertical locations where $\bar{T} = T_m$ and where $\bar{T} = 1 - T_m$, respectively. This definition of the thermocline thickness is illustrated in Fig. 2.

The quantity y_m is another important characteristic of the vertical temperature profile, because it relates directly to the amount of cold fluid in the tank at a given instant. We denote this cold-fluid volume by ϕ and define it as the amount of cold liquid at a temperature less than T_m. The cold-fluid volume is

$$\phi = y_m X = t - \delta X \tag{9}$$

for the ideal, one-dimensional model.

Using the definition given in Eq. (8) and the analytic solution without mixing ($\kappa = 1$), the thermocline thickness grows according to

$$\delta = 2(t/\mathrm{Pe})^{1/2} f(T_m), \tag{10}$$

where $f(T_m) \equiv \mathrm{erfc}^{-1}(2T_m)$. Since the function f is smooth for the interval of interest, $T_m = (0.05, 0.25)$, a quadratic, least-squares fit provides an excellent approximation. The fitted equation is

$$f(T_m) = 1.46 - 0.36(33.2T_m - 1.0)^{1/2}. \tag{11}$$

This equation, in combination with Eq. (10), provides a convenient method for estimating the thermocline thickness in the ideal limit of simple one-dimensional conduction.

The other important type of data measured for thermal storage tanks are the time traces of the inlet and outlet fluid temperature. For these data, the important feature is the time at which the outlet temperature, T_o, either drops to, or rises to, T_m for the charging or discharging process, respectively. We refer to these two times as the charging time, t_c, and the discharging time, t_d. The importance of the discharge time has been recognized not only in the chilled-water storage community where it was originally referred to as the 'useful volume' by Wildin and Truman (1985), but also in the solar–thermal community where it was termed the 'discharge efficiency' by Lavan and Thompson (1977).

For the one-dimensional model, the outlet-temperature history for the charging process is $T_o(t) = \bar{T}(Y,t)$ and the charging time, t_c, is given implicitly by

$$T_o(t_c) = T_m = 1 - (1/2)\,\mathrm{erfc}\left[\frac{Y - t_c/X}{2(\kappa t_c/\mathrm{Pe})^{1/2}}\right]. \tag{12}$$

For typical design and operating conditions, the ideal charging time is less than 1.1 tank volumes. Of course, in reality, the thermocline is generally thicker than that predicted by the ideal model, and more cold fluid must be put into the tank in order to push out the thermocline. Likewise, for the discharging process, the actual volume of cold fluid that can be removed from the tank is usually less than predicted by the ideal model.

The most important overall measure of thermal performance is the efficiency of the stratified storage tank. The efficiency of a stratified storage device is the ratio of energy added during the discharging process, $\hat{Q}_d$, to that removed during the charging process, $\hat{Q}_c$. We define these two quantities, in dimensionless terms, as

$$Q_d \equiv \frac{\hat{Q}_d}{\rho c V \Delta\hat{T}} = \int_0^{t_d} [1 - T_o(t)]\,\mathrm{d}t. \tag{13a}$$

and

$$Q_c \equiv \frac{\hat{Q}_c}{\rho c V \Delta\hat{T}} = \int_0^{t_c} T_o(t)\,\mathrm{d}t, \tag{13b}$$

where T_o is a suitably-averaged outlet temperature and $\Delta\hat{T}$ is the difference between the initial uniform temperature in the tank and the steady inlet temperature for both the discharging and the charging process. The upper limits of the integrals in Eqs. (13a) and (13b) are the discharging and charging times already mentioned. As discussed in our earlier paper (Homan et al., 1996), the above definition of the efficiency corresponds to a fully charged condition and accounts for the constraints on the outlet temperature dictated by the cooling function of the system. For the one-dimensional model, the quantity Q_c is approximately equal to unity, irrespective of Pe. For this reason, the efficiency of the stratified storage tank depends primarily on Q_d. The efficiency of the overall, storage-based cooling system depends strongly on the charging time however, since it corresponds to increased chiller run-time.

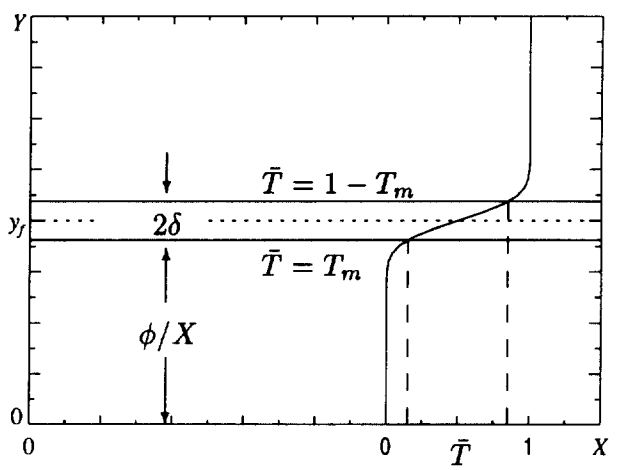

Fig. 2. Definition of parameters describing the size and location of the thermocline for a one-dimensional temperature distribution.

3. Results and discussion

We present results for a fixed set of flow parameters chosen as Re = 50, Pr = 10, and Fr = 1. These values correspond to a relatively slow filling process that is strongly influenced by the stratification. The Prandtl number is representative of water at approximately 10°C. With the flow parameters fixed, we concentrate on the influence of changes in geometry. In the first subsection here, we examine the charging of a tall tank, making explicit the comparison to the analytic, one-dimensional model. In the second subsection, we present results for the charging and discharging of a square tank and its computed efficiency.

3.1. Tall-tank limit

The charging of a tall tank, as illustrated in Fig. 1(a), produces a wide range of fascinating buoyant-flow phenomena. Initially, the inflow of cold liquid produces a gravity current which moves across the bottom of the tank at a nearly uniform

velocity and creates the initial thermocline. The gravity current slows as it approaches the right vertical wall and then collides with it. The collision causes some cold liquid first to bounce up along the wall and then to collapse downward, exciting a complex array of internal wave phenomena. These waves are evident in oscillations of the thermocline and persist for a long time. As the filling process continues, the thermocline is transported vertically away from the inlet, and the flow pattern below the thermocline transitions from a multicell recirculation pattern to one dominated by a single large vortex above the inlet. Further description of these stages may be found in our earlier paper (Homan and Soo, 1997).

The centerline temperature profiles shown in Fig. 3 illustrate the growth and vertical transport of the thermocline during the filling process. One of the most striking features of this plot is the nonequilibrium condition evident in the profile at $t = 64$. This profile is a result of the strong convective motion produced by the jet inflow. This effect appears even more clearly in a plot of vertical profiles at selected positions across the tank width. Fig. 4 shows such a set of profiles at time $t = 128$. At this instant of time, the jet vortex is centered at $x \simeq 5.5$ with a diameter of approximately 2.5. The counterclockwise motion of the jet vortex has noticeably widened the lower portion of the thermocline as evident in the $x = 2$ profile. The profiles for $x \geqslant 8$ appear to be only slightly influenced by the velocity field since, at this stage of the charging process, this region contains only relatively low fluid velocities.

As introduced in the formulation section, one way of measuring the thermal mixing is to compute the accumulation of 'cold' fluid in the storage tank. For the two-dimensional model, we compute the cold volume from

$$\phi \equiv \frac{\hat{\phi}}{l^2} = \int_0^Y \int_0^X \mathscr{H}[T_m - T(x,y,t)]\,dx\,dy, \tag{14}$$

where the Heaviside function $\mathscr{H}$ is defined as

$$\mathscr{H}[T_m - T(x,y,t)] \equiv \begin{cases} 0, & T(x,y,t) \geqslant T_m, \\ 1, & T(x,y,t) < T_m. \end{cases} \tag{15}$$

Numerically, we evaluate the integral appearing in Eq. (14) using the trapezoidal rule. In addition to the ideal model,

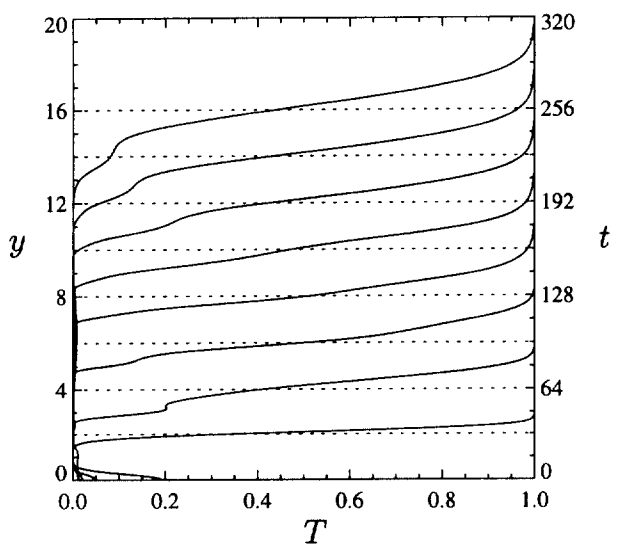

Fig. 3. Time series of temperature profiles at the tank centerline, $x = X/2$, for the tall-tank case with $X = 16$.

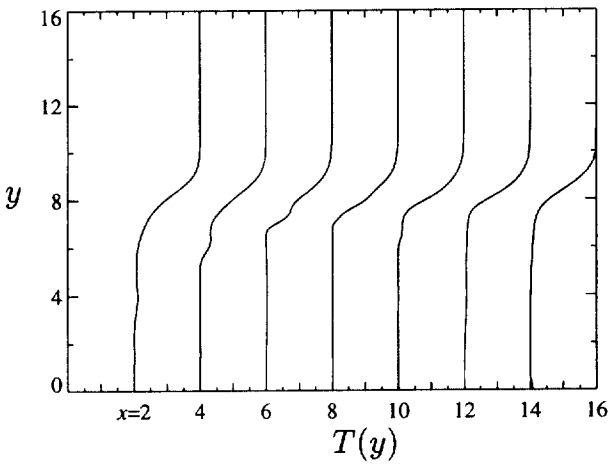

Fig. 4. Vertical profiles of temperature at $t = 128$ for the charging of a tall tank with $X = 16$.

one obvious standard for comparison with the cold volume is the cumulative amount of cold fluid put into the tank,

$$\phi_i(t) \equiv \frac{\hat{\phi}_i}{l^2} = \int_0^t dt \int_0^1 u(0,y,t)\,\mathscr{H}[T_m - T(0,y,t)]\,dy. \tag{16}$$

since the inlet velocity and temperature are steady for all time except the relatively small startup period, $\phi_i(t) \cong t$.

Fig. 5 shows time traces of the cold volume calculated for three representative values of T_m. For $T_m = 0.05$ and 0.15, the cold volume increases slowly for $t \leqslant 64$ and then starts to increase with time at a rate almost equal to unity. The opposite seems to be true for $T_m = 0.25$; the rate of increase actually appears to decrease with time. The explanation is that in the early stages of the charge process, much of the thermal mixing actually increases the cold volume inventory if $T_m \leqslant 0.25$ is used as the criterion. At later times, when the growth of the thermocline is attributable more to conduction than to convective mixing, its growth rate coincides with that of the smaller T_m.

The shape of the curves shown in Fig. 5 are remarkably similar to those presented by Baines et al. (1982, 1983) in their study of filling a tank of fresh water with salt water. In their study, the concentration gradient was visualized by a

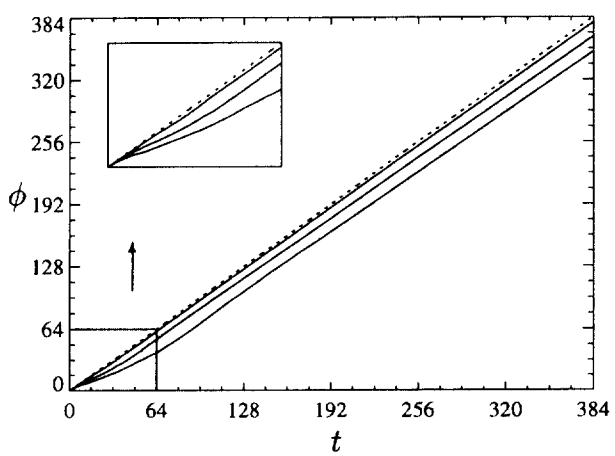

Fig. 5. Time variation of cold volume during the charging of a tall tank with $X = 16$ for $T_m = 0.05$, 0.15 and 0.25 (solid lines) from bottom to top, respectively. The dashed line indicates $\phi = t$.

shadowgraph technique and the volume under it computed at a series of times during the filling process. They assumed this volume corresponded to the amount of fluid at a salinity level approximately equal to that of the inlet. Since they did not indicate how the interface they measured with the shadowgraph technique correlated with density, quantitative comparison with their results is difficult. However, the basic shape of the $T_m = 0.05$ and 0.15 curves in Fig. 5, showing an initial transient in which ϕ increases at a sublinear rate and then approaches a linear increase with time, is certainly evident in their findings. Also evident in some of their data is behavior close to that seen in the curve for $T_m = 0.25$.

The computed temperature field may also be used to calculate an effective diffusivity. As already suggested, the in-tank temperature field can be related to an effective diffusivity either through the thermocline thickness or the cold volume. Note that this results in a value for the effective diffusivity that is, in a sense, averaged over both space and time. This is in contrast to a direct computation of the diffusivity from the perturbation integral appearing in Eq. (4). From Eq. (10), the mixing factor is related to the thermocline thickness by

$$\kappa \equiv 1 + \varepsilon/\alpha = \frac{\mathrm{Pe}}{4t}\left(\frac{\delta}{f}\right)^2, \tag{17}$$

and to the cold volume by

$$\kappa \equiv 1 + \varepsilon/\alpha = \frac{\mathrm{Pe}}{4t}\left(\frac{t-\phi}{Xf}\right)^2. \tag{18}$$

The thermal mixing factor computed by these two methods may differ however. The correspondence will depend on how closely $\delta = (t - \phi)/X$ in the two-dimensional temperature field. Since, in the analytic model, the thermocline thickness and height y_m are not functions of x, their counterparts in the two-dimensional case must be representative of the local quantities illustrated in Fig. 6.

A comparison of these quantities averaged over the width of the tank and at the tank centerline, $x = X/2$, is shown in Table 1. The table shows that for the parameters presently under consideration, estimation of the mixing factor by the horizontally-averaged thermocline thickness or the cold volume is essentially equivalent, i.e., $\bar{\delta} \sim (t - \phi)/X$. It also indicates that estimating the mixing factor from a single vertical profile of temperature at the tank centerline would be quite adequate, since $y_m(x = X/2) \sim t/X - \delta(x = X/2)$.

Although the relationships between δ, y_m, and ϕ in the one-dimensional model seem to hold roughly true in the two-dimensional model, their slight differences are equally important, since they give clues as to the shape of the overall thermocline. For example, at $t = 64$, the horizontally averaged thermocline thickness is less than the local thickness at the tank centerline. However, at later times, the relationship reverses. The explanation is that at $t = 64$, the local thickness is dictated by the convective motion of the jet vortex and internal gravity waves. A similar result would also be obtained if, for example, a profile

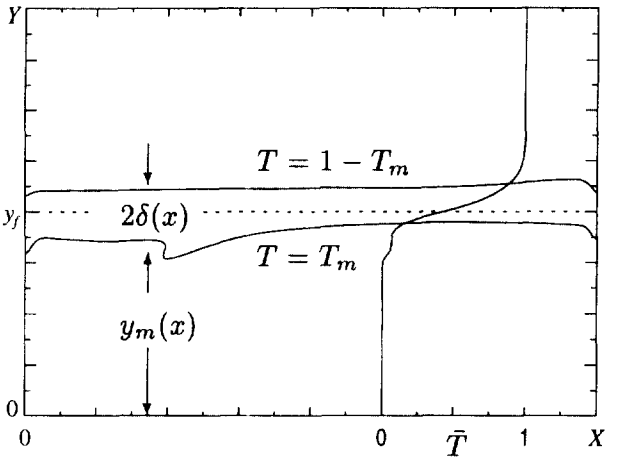

Fig. 6. Parameter definitions for a two-dimensional temperature distribution.

were taken at a horizontal position that cut through the bump in the lower edge of the thermocline shown in Fig. 6. The same observations can also be made for a comparison between $y_m(X/2)$ and ϕ/X. Of course, there are also horizontal positions where the opposite is true. A local thickness less than the average is most pronounced directly above the center of the jet vortex. Inferences about the flowfield can even be made from a single temperature profile, without direct knowledge of $\bar{\delta}$ or ϕ. In that case, comparison of $t/X - y_m$ with $y_m - t/X$ indicates whether the thermocline thickness is symmetric about the fill line, $y_f \equiv t/X$. A mismatch between the two quantities is evidence that the thermocline is still under the influence of the high fluid velocities present in the near inlet region. Once the thermocline has moved a sufficient distance away from the inlet, the thermocline becomes almost exactly symmetric.

We have chosen to compute the mixing factor based on the cold volume, ϕ, since it avoids the ambiguity of determining a thermocline thickness at instants when the profile is not a single-valued function of the vertical coordinate y. The time trace of the diffusivity ratio calculated in such manner is shown in Fig. 7. Interestingly, the ratio is negative for $T_m = 0.25$, which means less 'cold' water is being consumed than for conduction alone, since convective mixing is producing more fluid at a temperature that satisfies the maximum-temperature criterion.

A doubling of the domain width produces a noticeable change in the level of thermal mixing. For example, at $t = 256$, $\phi \simeq 224$ for $X = 16$; whereas, for $X = 32$, $\phi \simeq 192$. Since $t - \phi$ for $X = 32$ is approximately twice that for $X = 16$, the explanation for much of the increased thermal mixing must be thermal diffusion across the increased cross-sectional area of the thermocline. This is confirmed by a comparison of the mixing factor for these two cases, as shown in

Table 1
Comparison of local and average parameters that provide some measure of thermal mixing; data are from the tall-tank case with $X = 16$, $Y_\infty = 32$, and $T_m = 0.15$

t	$\bar{\delta}$	$\delta(X/2)$	$y_m(X/2)$	ϕ	$(t-\phi)/X$	$t/X - \delta(X/2)$
64	0.66	0.88	3.03	53.6	0.65	3.12
128	1.07	0.78	7.39	116	0.75	7.22
192	1.17	1.13	10.9	177	0.94	10.9
256	1.19	1.13	15.1	240	1.00	14.9
320	1.26	1.25	18.9	302	1.13	18.8
384	1.35	1.38	22.8	364	1.25	22.6

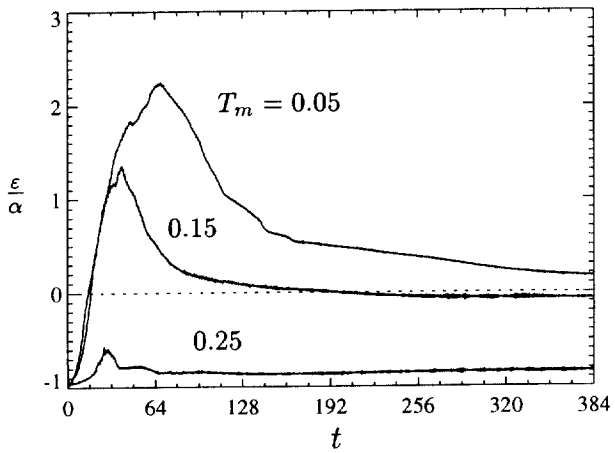

Fig. 7. Variation of diffusivity ratio with time for the tall-tank case with $X = 16$.

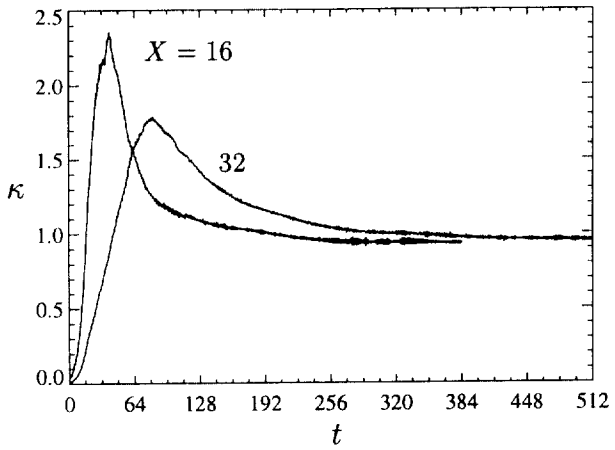

Fig. 8. Time trace of the mixing factors for a tall tank with $X = 16$ and $X = 32$. Both curves are for $T_m = 0.15$.

Fig. 8. At $t = 350$, for example, the mixing factors are nearly the same. The shapes of the curves differ, however, in two important regards: (1) the peak of the $X = 16$ curve is over one-third higher than that of the $X = 32$ curve; and (2) the peak of the $X = 32$ curve does not fall off as rapidly as in the $X = 16$ case. We believe these differences can, in large part, be attributed to changes in the kinetic energy of the gravity current when turned at the tank wall and the thermocline residence time near the high velocities present in the inlet region.

The present results lie in a Reynolds number range that has been investigated both experimentally and computationally by previous researchers. Mixing factors estimated from their results are shown in Table 2. For the data of Wildin and Sohn (1993), the mixing factor has been estimated from vertical temperature profiles measured during the charging of a rectangular tank ($H \times W = 0.91$ m $\times$ 2.4 m) with a single inlet of either 1.5 or 2.5cm in height. For the computational results presented by Valentine and Tannous (1985), the mixing factor has been estimated from centerline temperature profiles. The numerical scheme of Valentine and Tannous is first-order accurate in space. Computational data for a tank with a single corner inlet have also been presented by Cai et al. (1993) and Stewart et al. (1994), based on a two-equation turbulence model and a numerical method of first-order spatial accuracy. The mixing factor has been estimated from contour plots of two-dimensional temperature presented in the two works. Fig. 9 shows the data of Table 2 with Reynolds number along the abscissa. The close correspondence of the present results to the experimental trend of Wildin and Sohn provides strong support for the accuracy of our model and of the need to resolve the small thermal interior layers.

3.2. Square tank

The rather surprising result of imposing an upper boundary, specifically a zero-shear stress boundary, is that it has relatively little effect on the thermocline and the inlet flowfield beneath it, at least until very late in the filling process. Table 3

Table 2
Estimated mixing factors based on numerical and experimental data for the filling of a rectangular tank with a single inlet; the mixing factor, κ, was computed from vertical profiles of temperature using $\phi \simeq y_m(x)X$ and $\overline{\delta} \simeq \delta(x)$ for the data of Valentine and Tannous (1985) and Wildin and Sohn (1993); all mixing factors are based on $T_m = 0.15$

	$\kappa(\phi)$	$\kappa(\delta)$	t/X	Re	Pr	Fr	W/l	H/W	$l/\Delta x$
Tall-tank limit	1.0	1.6	12.0	50	10	1.0	16	2.0	16
	1.1	1.7	12.0	50	10	1.0	16	2.0	32
	1.2	2.2	6.0	50	10	1.0	32	1.0	16
Square tank	1.1	1.7	12.0	50	10	1.0	16	1.0	32
Cai et al. (1993)	200.0	230.0	11.0	333	12	0.08	10	2.0	4
Stewart et al. (1994)	70.0	100.0	5.3	167	12	0.15	10	2.0	4
	280.0	310.0	7.1	333	12	0.08	15	1.3	4
Valentine and Tannous (1985)	18.0	32.0	2.4	100	10	0.43	15	0.67	2
	–	20.0	5.3	100	10	0.43	15	0.67	2
Wildin and Sohn (1993)	2.3	2.4	11.0	159	9	0.77	155	0.38	–
(experimental)	1.8	1.8	33.0	159	9	0.77	155	0.38	–
	2.2	2.9	7.3	191	9	0.42	95	0.38	–
	0.9	2.1	21.0	191	9	0.42	95	0.38	–
	7.1	11.0	11.0	316	9	1.47	155	0.38	–
	7.5	8.7	23.0	316	9	1.47	155	0.38	–
	23.0	19.0	11.0	429	9	2.02	155	0.38	–
	12.0	17.0	23.0	429	9	2.02	155	0.38	–
	27.0	21.0	6.5	446	9	0.99	95	0.38	–
	18.0	22.0	20.0	446	9	0.99	95	0.38	–

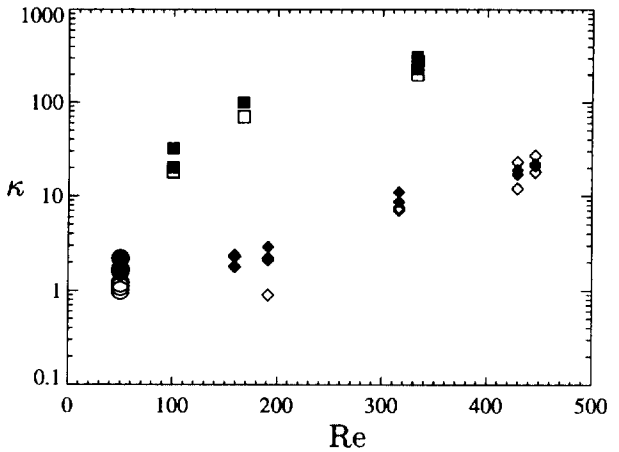

Fig. 9. Comparison of mixing factors predicted numerically and experimentally for a rectangular tank with a single inlet and outlet. The data are (1) the present results (○), (2) previous computational results (□) of Cai et al. (1993), Stewart et al. (1994) and Valentine and Tannous (1985), and (3) empirical results (◇) of Wildin and Sohn (1993). Open symbols denote $\kappa(\phi)$ and filled symbols $\kappa(\delta)$.

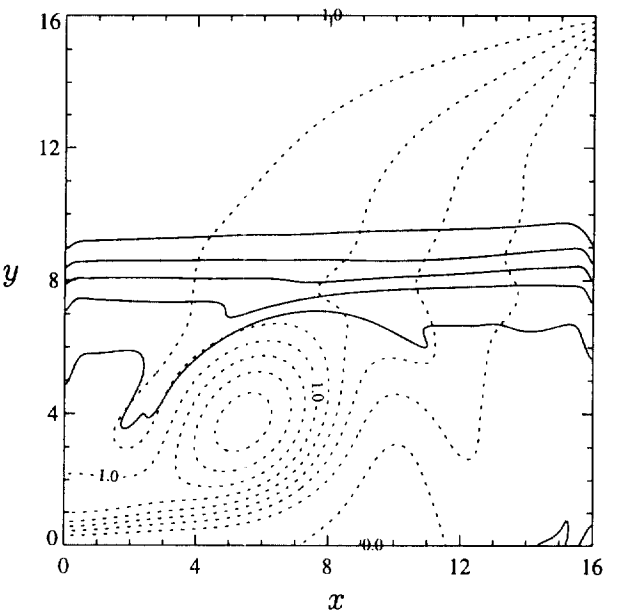

Fig. 10. Isotherms ($T=0.05$, 0.25, 0.5, 0.75, 0.95) overlayed with instantaneous streamlines ($\Delta\psi = 0.2$) at the midpoint, $t = XY/2 = 128$, of the charging process for a square tank.

shows a comparison of salient parameters for the tall-tank and finite-height cases. Apparently, at these Reynolds and Froude numbers, the thermocline functions very effectively in isolating the flowfields above and below it. Instantaneous streamline and temperature contours, shown in Fig. 10, also illustrate this effect clearly.

A plot of the cold volume, shown in Fig. 11, reveals very little influence of the tank height until about the last one-sixteenth of the tank volume. At that point, the cold volume levels off as the remaining portion of the thermocline becomes trapped in the upper corner opposite the inlet. The higher T_m curve begins to level off first because more of the thermocline meets the criterion for being 'cold', thus the withdrawal of the thermocline provides no net gain in cold volume, since fluid flows into the tank at a rate identical to which it flows out of the tank.

The outlet temperature history for this same case, shown in Fig. 12, seems quite smooth, similar to a profile for the one-dimensional, pure conduction model as given by Eq. (7). The fact that the bulk-averaged and outlet-centerline profiles do not coincide is evidence of the upward movement of the thermocline late into the filling process. For $T_m = 0.15$, the bulk-averaged outlet temperature rises above T_m at time $t_c = 278.4$. Relative to the overall tank volume, the charging fraction is $t_c/XY = 278.9/256 = 1.09$.

This charging time can also be used to compute a mixing factor from

$$\kappa = \frac{\mathrm{Pe}}{4t_c}\left(\frac{t_c/X - Y}{f}\right)^2. \tag{19}$$

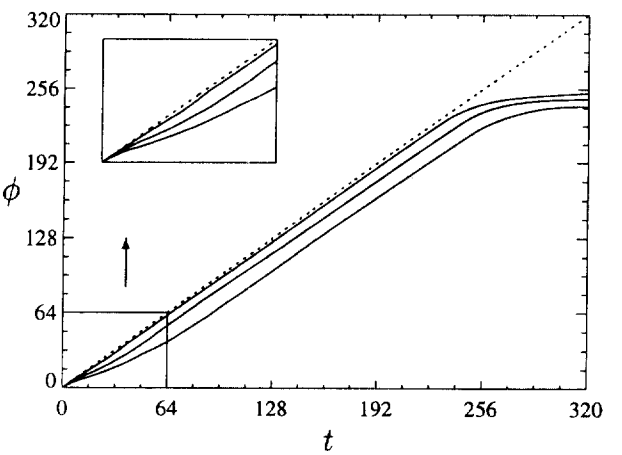

Fig. 11. Time variation of cold volume during the charging of a tank with $X = Y = 16$ for $T_m = 0.05$, 0.15 and 0.25 (solid lines) from bottom to top, respectively. The dashed line indicates $\phi = t$.

The mixing factor based on the charging time is $\kappa(t_c) = 1.7$. This value is comparable to that determined by the interior mixing factor, since for example, at $t = 224$, $\kappa = 1.1$ for both the tall and square-tank case.

Table 3
Measures of thermal mixing at select stages of the charge process for the tall-tank limit and square tank ($T_m = 0.15$)

	$t = 64$			$t = 128$			$t = 224$		
	$\bar{\delta}$	ϕ	κ	$\bar{\delta}$	ϕ	κ	$\bar{\delta}$	ϕ	κ
$X = 16, Y_\infty = 32$	0.68	52.9	1.7	1.13	115	1.2	1.13	208	1.1
$X = 32, Y_\infty = 32$	0.52	42.8	1.6	0.72	99.7	1.4	1.35	191	1.1
$X = 16, Y = 16$	0.67	52.9	1.74	1.1	115	1.2	0.96	208	1.1

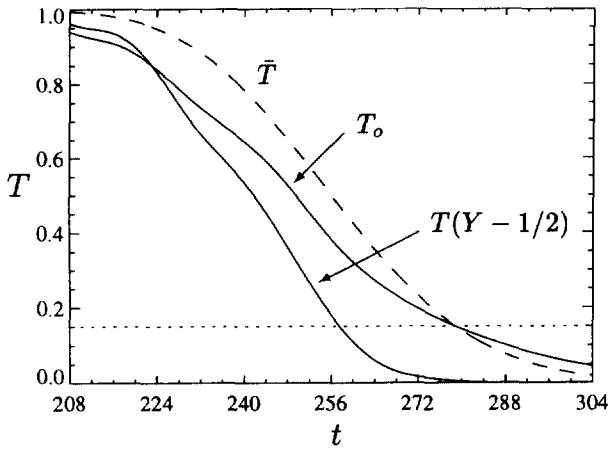

Fig. 12. Time trace of outlet fluid temperature for charging of a tank with $X = Y = 16$.

The slight oscillations in outlet temperature evident in Fig. 12 are a remnant of the internal waves set off by the turning of the gravity current early in the charging process. As a side note, computations we have done for a tank aspect ratio (H/W) of one-half show that the oscillations are even larger, since the thermocline approaches the outlet in half the time. Oscillations of tank outlet temperature, similar in character to our numerical results, have also been observed in discharging experiments conducted by Wildin (1989).

For the discharging process, warm liquid flows into the tank through the slot adjacent to the free surface, and cold fluid is drawn out from the bottom of the tank. Fig. 13 contains the streamlines and temperature contours midway through the discharging process and at the end of the discharging process. The recirculation pattern above the thermocline reveals an obvious change from that observed below the thermocline in the charging process. During the charging process, the primary vortex did not move close to the wall opposite the inlet until very late in the process. In contrast, for the discharging process, the absence of a shear stress along the free surface allows the jet inertia to place the main recirculation cell right up against the left wall. The free surface also leads to higher amplitude internal waves and allows for a significantly stronger jet vortex. Surprisingly, the resulting thermocline thickness, at $t = 192$ for example, is only 1 or 2% larger at the same time in the charging process. Apparently, the stronger oscillations do not lead to large increases in the level of thermal mixing.

The discharging time t_d for the case $X = Y = 16$ is 0.87 for $T_m = 0.15$. The discharging time can be used to estimate an equivalent mixing factor using

$$\kappa = \frac{\mathrm{Pe}}{4t_d}\left(\frac{Y - t_d/X}{f}\right)^2. \tag{20}$$

The mixing factor computed from Eq. (20) is $\kappa(t_d) = 4.8$. Although as indicated earlier, the thermocline thicknesses at an intermediate time in the charging and discharging processes are approximately equal, the discharging time indicates a higher effective diffusivity than that observed for the charging process. The explanation for this apparent discrepancy is that more of the thermocline is trapped at the bottom of the tank at the end of the discharging process than is caught at the upper surface at the end of charging.

Starting from a uniform initial condition for both the charging and the discharging process, the charge heat transfer is 247.4, and the discharge heat transfer is 210.6, as computed from a trapezoidal rule integration of the bulk-averaged outlet temperature. The efficiency, Q_d/Q_c, is therefore 0.85, only a few percent less than the ideal, pure-conduction efficiency at $\mathrm{Pe} = 500$ of $\eta = 0.925$ (Homan et al., 1996).

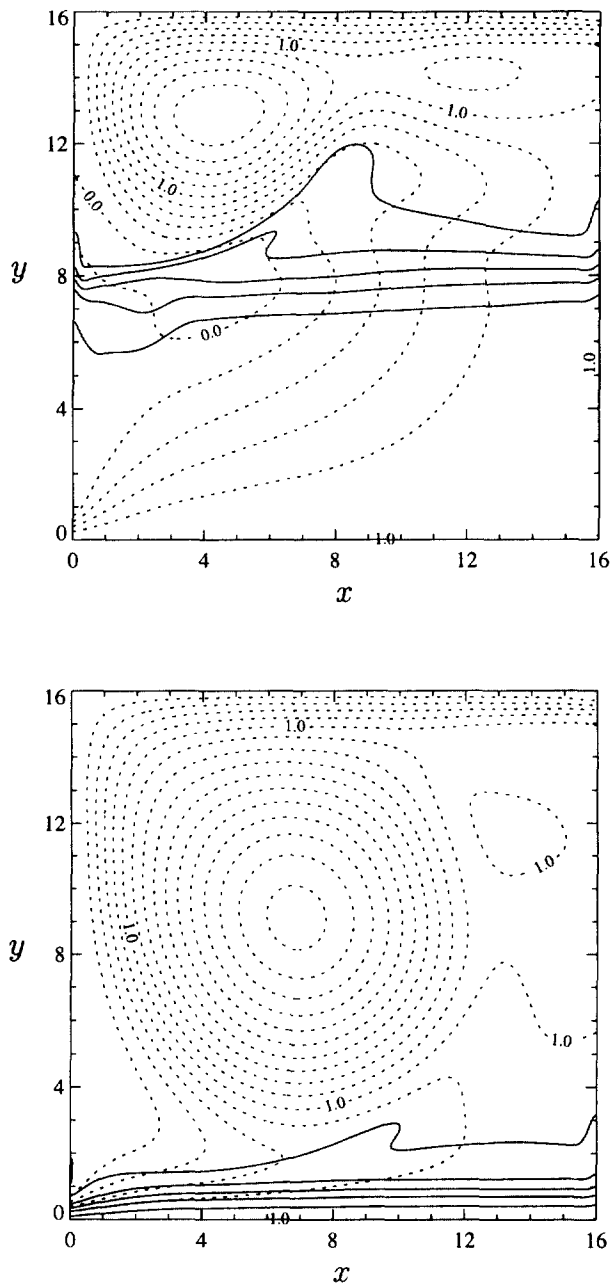

Fig. 13. Isotherms ($T = 0.05$, 0.25, 0.5, 0.75, 0.95) overlayed with instantaneous streamlines ($\Delta\psi = 0.2$) for two instants, $t = 128$ and 256, during the discharging of a tank with $X = Y = 16$.

4. Conclusions

In this paper, we have shown that two-dimensional numerical simulations of the filling of a stratified storage tank with a single inlet and outlet exhibit excellent quantitative agreement with experimental data when the thermal interior layers are adequately resolved. Resolving the thermal layers is important not only for quantifying the level of thermal mixing but also for capturing the transients driven by the action of gravity

on the unsteady temperature field. For the laminar flows simulated, the computed efficiency of the full charge and discharge cycle is within 10% of the ideal limit predicted by a one-dimensional model.

Recognizing the one-dimensional model as the evolution equation of the horizontally averaged temperature field, we have cast the deviation from one-dimensional motion into the product of an effective diffusivity and the vertical gradient in mean temperature. This diffusivity has enormous practical utility even when assumed to be spatially uniform. In contrast to storage-tank efficiency that has a single value for the complete charging and discharging process, the effective diffusivity factor can be used to quantify the level of thermal mixing at any stage of the charging and/or discharging process. The diffusivity factor can also be simply estimated from minimal experimental or computational data, i.e., vertical temperature profiles or time traces of tank outlet temperature. Analysis of our two-dimensional data reveals that the most important transients are, in order of importance: (1) the removal of the thermocline at the end of the discharging and charging processes and (2) the initial formation of the thermocline at the beginning of the discharging and charging processes. Since chilled-water storage tanks are often discharged at a faster rate than which they are charged, the discharging process could, in general, be even more important than indicated by the present results.

Acknowledgements

This research was supported by the US Army Construction Engineering Research Laboratories of Champaign, IL, through the AT23-EB-ESO Program. Computing time on the SGI Challenge has been provided by a grant from the National Center for Supercomputing Applications (NCSA) of Urbana, IL. The reviews and helpful discussions provided by Professor John S. Walker are gratefully acknowledged.

References

Baines, W.D., Martin, W.W., Sinclair, L.A., 1982. On the design of stratified thermal storage tanks. ASHRAE Trans. 88, 426–439.

Baines, W.D., Martin, W.W., Smith, D.M., 1983. Development of stratification in a rectangular tank by horizontal inflow. J. Fluids Eng. 105, 59–64.

Cai, L., Stewart, W.E., Jr., Sohn, C.W., 1993. Turbulent buoyant flows into a 2-D storage tank. Int. J. Heat Mass Transfer 36, 4247–4256.

Chan, A.M.C., Smereka, P.S., Giusti, D., 1983. A numerical study of transient mixed-convection flows in a thermal storage tank. J. Solar Energy Eng. 105, 246–253.

Cole, R.L., Bellinger, F.O., 1982. Thermally stratified tanks. ASHRAE Trans. 88, 1005–1017.

Homan, K.O., Soo, S.L., 1997. Model of the transient stratified flow into a chilled-water storage tank. Int. J. Heat Mass Transfer (accepted for publication).

Homan, K.O., Sohn, C.W., Soo, S.L., 1996. Thermal performance of stratified chilled water storage tanks. Int. J. HVAC and R Res. 2, 158–170.

Lavan, Z., Thompson, J., 1977. Experimental study of thermally stratified hot water storage tanks. Solar Energy 19, 519–524.

Oppel, F.J., Yoon, H.K., Ghajar, A.J., Moretti, P.M., 1985. Computer Simulation for Stratified Thermal Storage. Proceedings of the Symposium on Modeling Environmental Flows, ASCE/ASME Mechanics Conference, pp. 127–135.

Seeley, R.S., 1996. District cooling gets hot. Mech. Eng. 118, 82–84.

Stewart, W.E., Jr., Cai, L., Sohn, C.W., 1994. Thermal stratification of chilled-water slot flows into storage tanks. ASHRAE Trans. 100, 305–317.

Truman, C.R., Wildin, M.W., 1989. Finite difference model for heat transfer in stratified thermal storage tank with throughflow. Proceedings of the ASME/AICHE National Heat Transfer Conference, vol.110, 45–55.

Truman, C.R., Roybal, L.G., Wildin, M.W., 1985. A finite difference model for stratified chilled-water thermal storage tanks. Proceedings/Communications of Enerstock85, Toronto, Canada, pp. 613–617.

Valentine, D.T., Tannous, A.G., 1985. Stratification of a two-dimensional reservoir produced by a buoyant inflow. Proceedings of the Symposium on Modeling Environmental Flows, ASCE/ASME Mechanics Conference, pp. 111–117.

Wendland, R.D., Blatt, M.H., 1992. Reliable and efficient: Cool storage meets the challenges of the '90s. Electricity J. 5, 58–63.

Wildin, M.W., 1989. Performance of stratified vertical cylindrical thermal storage tanks. Part II: Prototype tank. ASHRAE Trans. 95, 73–82.

Wildin, M.W., Sohn, C.W., 1993. Flow and temperature distribution in a naturally stratified thermal storage tank. USACERL TR FE-94/01, US Army Construction Engineering Research Laboratories.

Wildin, M.W., Truman, C.R., 1985. A summary of experience with stratified chilled water tanks. ASHRAE Trans. 92, 956–976.

Zurigat, Y.H., Liche, P.R., Ghajar, A.J., 1991. Influence of inlet geometry on mixing in thermocline thermal energy storage. Int. J. Heat Mass Transfer 34, 115–125.